Available online at www.sciencedirect.com
ScienceDirect
Geochimica et Cosmochimica Acta 71 (2007) 5313–5324
Geochimica et Cosmochimica Acta
www.elsevier.com/locate/gca

Interfacial water structure on the (0 1 2) surface of hematite: Ordering and reactivity in comparison with corundum

Jeffrey G. Catalano *, Paul Fenter, Changyong Park

Chemistry Division, Argonne National Laboratory, 9700 South Cass Avenue, Argonne, IL 60439, USA

Received 3 July 2007; accepted in revised form 20 September 2007; available onilne 29 September 2007

Abstract

Many geochemical reactions that control the composition of natural waters, contaminant fate and transport, and biogeochemical element cycling take place at the interface between minerals and aqueous solutions. A fundamental understanding of these important processes requires knowledge of the structure of mineral–water interfaces. High-resolution specular X-ray reflectivity was used to determine the structure of the hematite (0 1 2)–water interface. Relaxation of the surface was observed to be minor, and water was found to order near the hematite surface. Two sites of adsorbed water are inferred to be ordered laterally, one bridging between triply coordinated functional groups and the other bridging between the singly coordinated functional groups on the surface, as steric constraints limit the possible arrangements of water molecules occurring at the observed heights above the hematite surface. Relaxations of the hematite and corundum (0 1 2) surfaces, which are isostructural, are similar and limited primarily to the top most layer of the structures. No significant changes to the interfacial stoichiometry (i.e., partial occupancy of surface species) are observed in either case. The structure of interfacial water is similar on the hematite and corundum (0 1 2) surfaces as well, although water appeared to be less well ordered on the hematite surface. This may be due to expected differences in the oxygen exchange rates from surface functional groups or the apparent better matching of the corundum oxygen lattice to the natural structural ordering in water, and suggests that the dielectric constant gradients of interfacial water may differ on the two surfaces. Similar charging behavior is expected for these surfaces as similar types of surface functional groups are exposed. Although generally similar, subtle differences in the reactivity of hematite and corundum (0 1 2) surfaces to arsenate adsorption, and possibly the adsorption of other species, may be related to the difference in ordering of interfacial water observed in this study.

1. INTRODUCTION

The interface between a mineral and aqueous solution is a chemical and structural transition region where many important geochemical reactions occur, such as adsorption and desorption, precipitation and dissolution, and heterogeneous oxidation and reduction (Brown, 2001; Al-Abadleh and Grassian, 2003). Surface complexation models created to describe and predict such reactions incorporate molecular-level aspects of mineral–water interfaces, as they assume an explicit double layer structure (Hayes and Leckie, 1987; Hayes et al., 1988; Hiemstra et al., 1989; Davis and Kent, 1990; Sverjensky, 1993; Hiemstra and van Riemsdijk, 1996; Machesky et al., 2001). Water in the mineral–aqueous solution interfacial region often displays molecular-level ordering that decays away from the mineral surface (Israelachvili and Pashley, 1983; Fenter and Sturchio, 2004). It is important to characterize the structure of the interfacial regions of specific crystallographic mineral surfaces in order to gain a systematic understanding of the physical and chemical properties of this transition zone. In addition, such systems are ideal for studying fundamental aspects of ion adsorption reactions (e.g., Bargar et al., 2004; Zhang et al., 2004, 2006a,b; Catalano et al., 2005, 2006a, 2007;

* Corresponding author. Present address: Department of Earth and Planetary Sciences, Washington University, Campus Box 1169, Saint Louis, MO 63130-4862, USA. Tel.: +1 314 935 6015; fax: +1 314 935 7361.
E-mail address: catalano@wustl.edu (J.G. Catalano).

0016-7037/$ - see front matter © 2007 Elsevier Ltd. All rights reserved.
doi:10.1016/j.gca.2007.09.019

Waychunas et al., 2005; Park et al., 2006; Schlegel et al., 2006), which requires knowledge of the molecular-level structure of the surfaces being examined.

Surfaces of iron oxides such as hematite (α-Fe_2O_3) are of particular importance because of such minerals ability to adsorb trace elements, heavy metal, and radionuclides and to serve as terminal electron acceptors for dissimilatory iron-reducing bacteria (Brown et al., 1999). The structure of hydrated hematite (0 0 1) and (0 1 2) surfaces have been shown to only display minor relaxations compared to the bulk structure under ambient conditions (i.e., no reconstructions), although these surface may display variable terminations (Trainor et al., 2002, 2004; Catalano et al., 2006b, 2007; Tanwar et al., 2007a,b). Recent experimental and computation work has demonstrated that the exposed termination can nominally be controlled through specific preparation methods, especially on the (0 1 2) surface (Lo et al., 2007; Tanwar et al., 2007b).

In this study, we investigated the structure of the hematite (0 1 2)–water interface in situ using synchrotron-based high-resolution X-ray reflectivity. The hematite samples we examined were prepared in a way that produced a termination (Tanwar et al., 2007b) isostructural with the termination of the corundum (0 1 2) surface we recently characterized (Catalano et al., 2006b). Structural relaxations and ordering of interfacial water on the hematite (0 1 2) surface were characterized and then compared to that observed for the corundum (0 1 2) surface. This allows us to evaluate how differences in mineral composition and lattice parameters affect the hydration structure in the interfacial region.

2. MATERIALS AND METHODS

2.1. Sample preparation

Approximately 1 cm^2 natural hematite (α-Fe_2O_3) crystals, cut and polished parallel to the (0 1 2) surface plane, were obtained from Commercial Crystal Laboratories (Naples, FL). The crystals were cleaned prior to use; the cleaning procedure consisted of five alternating acetone and methanol rinses, followed by a deionized water (>18 MΩ cm) rinse. This was followed by a light base wash (10^{-3} M NaOH), light acid wash (10^{-3} M HCl), repeated deionized water rinsing, and drying with a jet of compressed N_2 gas. The samples were then annealed at 450 °C in air for 24 h. After cooling to 100 °C in the furnace, they were transferred to deionized water and stored there for one to three days prior to measurements.

2.2. X-ray reflectivity data collection

High-resolution specular X-ray reflectivity (XR) measurements of two separate hematite samples were performed at beamlines 20-ID-C (sample 1) and 11-ID-D (sample 2) at the Advanced Photon Source (APS). Measurements were made using a six-circle diffractometer with the incident X-ray beam energy selected by a cryogenically cooled Si (1 1 1) double-crystal monochromator on both beamlines. XR measurements (i.e., reflectivity versus momentum transfer, $Q = 4\pi \sin(\theta)/\lambda$) were made at 10.000 keV at 20-ID-C and 18.000 keV at 11-ID-D. Harmonic rejection and/or focusing were achieved through mirror systems specific to each beamline: a Rh-coated Kirkpatrick-Baez-type Si mirror was used at 20-ID-C for harmonic rejection; a Pt-coated Si mirror was used at 11-ID-D for vertical focusing and harmonic rejection. The reflected X-ray intensities were measured with a CCD area detector. The application of a CCD area detector to the measurement of XR, including data collection, data integration, and determination of statistical errors, has been described previously (Fenter et al., 2006). Samples were mounted in deionized water in a thin film geometry sample cell (Fenter, 2002) sealed with 8 μm thick Kapton™ plastic film. The cell was then mounted on a diffractometer for alignment and data collection.

2.3. X-ray reflectivity data analysis

The XR data were analyzed using previously described procedures (Fenter, 2002; Catalano et al., 2006b). The two datasets were fit simultaneously to the same structural model as a way to minimize the effects of possible systematic errors. Extrinsic factors, such as water film thickness (Fenter, 2002), roughness (Robinson, 1986), and a scale factor, were fit to each dataset. Also included in the fitting were the effects of sample miscut as described in Appendix A. The miscut rods contributing to each datapoint were identified from the CCD images and specified explicitly in the structure factor (i.e., scattering intensity) calculations. Although the effects of miscut on the XR differ little from the effects of roughness described by Robinson (1986), they were included in the calculation for completeness. Both crystals examined had a miscut angle of approximately 1°.

The structural model consisted of three Fe_2O_3 layers that were allowed to relax. Because of the resolution of the dataset, not all of the atomic positions in each layer could be refined independently without causing correlations between parameters, and some structural constraints were enforced. The lowest (highest) O atoms were constrained to have the same relaxations as the lowest (highest) Fe atoms in each layer since the individual positions were not resolved by the experimental data. The relaxations of the middle O atoms in the Fe_2O_3 layers were unconstrained. In the uppermost Fe_2O_3 layer, relaxation of both the middle and upper O atoms were unconstrained. The bulk crystal structure and vibrational amplitudes were taken from Finger and Hazen (1980). The structure was reindexed with an orthogonal P1 surface unit cell with the c-axis normal to the (0 1 2) surface having lattice parameters $|a_s| = 5.035$ Å, $|b_s| = 5.427$ Å, and $|c_s| = 7.364$ Å. The height scale used in all tables and figures was set to zero at the top of the uppermost Fe_2O_3 layer so that a consistent reference point was available throughout the analysis and discussion of the surface structure. Note that this height scale is different from that used by Catalano et al. (2006b) in the study of the corundum (0 1 2)–water interface; the comparable reference point in that study occurs at 17.40 Å.

Anomalous scattering factors for Fe and O (Cromer and Liberman, 1970; Waseda, 1984) were included in all struc-

ture factor calculations. The resulting electron density profile includes a spatial broadening term due to the finite resolution of the data (Fenter, 2002). As both datasets were collected to the same maximum Q ($Q_{max} = 5.46$ Å^{-1}), they had the same resolution ($\pi/Q_{max} = 0.58$ Å), and this value was used in the electron density profile calculation. The goodness-of-fit parameter (χ^2) and R-factor were calculated as follows:

$$\chi^2 = [1/(N-P)] \sum \left[(I - I_{calc})/\sigma_{exp}\right]^2 \quad (1)$$

$$R\text{-factor} = \sum [|I - I_{calc}|] \Big/ \sum [I] \quad (2)$$

where I is the measured intensities, I_{calc} is the intensities calculated from the model, σ_{exp} is the experimental uncertainties in the intensities, N is the number of data points, and P is the number of fitting parameters. All reported errors are based on the standard deviations obtained from the least squares fitting procedure and are reported at the 95% (2σ) confidence level. The uncertainties in individual data points are determined from counting statistics; estimated systematic errors determined from repeated measurements of fiducial points for each dataset (2.8% for sample 1 and 2.0% for sample 2) were added in quadrature to these uncertainties to better represent the expected reproducibility of the measurements.

3. RESULTS AND DISCUSSION

3.1. Analysis of XR data

Independent measurements of the specular XR of two unique hematite single crystals having the (0 1 2) surface orientation were made to confirm the reproducibility of the surface preparation and to minimize the effects of experimental systematic errors on the structure determination. Initial details of the interfacial water structure were evaluated through direct inversion of the experimental data using an error-correction algorithm (Fenter and Zhang, 2005). This type of analysis identifies density features in the interfacial region without the need to force-fit a structural model to the data, and is thus model-independent. However, it does require assumptions regarding the density/structure bounding the interfacial region; in this study we chose a fully occupied terminal Fe_2O_3 layer on the mineral side of the interface and featureless bulk water on the fluid side. We feel that these assumptions are well justified for this initial analysis as this termination of the hematite (0 1 2) surface has been observed on samples prepared similarly (Tanwar et al., 2007b), the XR displayed termination interference (Fenter and Park, 2004) features similar to those seen on a corundum (0 1 2) surface having an isostructural termination, and, although interfacial water is known to show ordering near an interface, the details of this ordering often depend on the structure of the crystallographic surface being examined, and we thus chose to avoid forcing any biased structural assumptions into this analysis.

Direct inversion of the data using these bounding assumptions reproduced the major features of the data (Fig. 1) even though an unrelaxed near-surface hematite structure was used. Two interfacial density features were

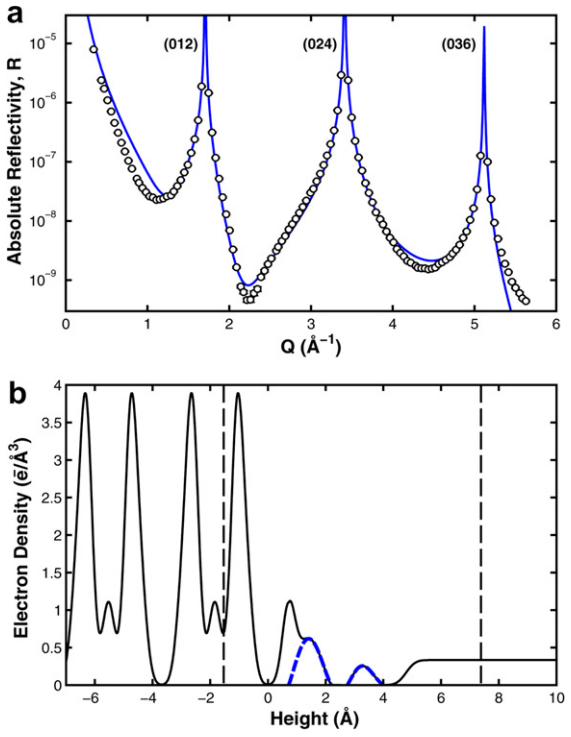

Fig. 1. Results of the direct inversion of the XR data for sample 2: (a) experimental XR data (circles) and XR calculated from the data inversion (line), (b) the resulting resolution-broadened interfacial density profile, including both the total density (solid) and the density added to the references structure (dashed) in the inversion process. The vertical dashed line in (b) delineates the window region where density could be added by the inversion algorithm. Results for sample 1 were nearly indistinguishable, and are thus not shown for clarity.

identified from this inversion process, occurring at 1.4 and 3.3 Å. Although inverted separately, both datasets produced nearly identical density features (only the sample 2 inversion is shown for clarity), with height differences of approximately 0.01 Å between the two inversions. This suggests that the features seen are intrinsic to the interfacial structure and not an artifact of systematic error in the data. Direct inversion of XR data for a similarly terminated corundum (0 1 2) surface produced density features at 1.6 and 3.2 Å, which were concluded to be from sites of adsorbed water (Catalano et al., 2006b). The isostructural nature of hematite and corundum suggests that the density features observed here have a similar origin.

A single structural model, described in Section 2.2, consistent with the interfacial density profile obtained through the direct inversion analysis was refined simultaneously versus the two datasets (Fig. 2). The resulting best-fit structural model (Table 1) fit the data well ($\chi^2 = 5.17$, R-factor = 0.045) and displayed minor relaxations (<0.1 Å) extending three Fe_2O_3 layers into the structure. As the relaxed atomic positions of the lowermost layer were statistical indistinguishable from the bulk atomic positions, relaxations deeper into the structure were not included in the refinement. Attempts were made to refine the occupancy of the uppermost Fe site, but the resulting values were al-

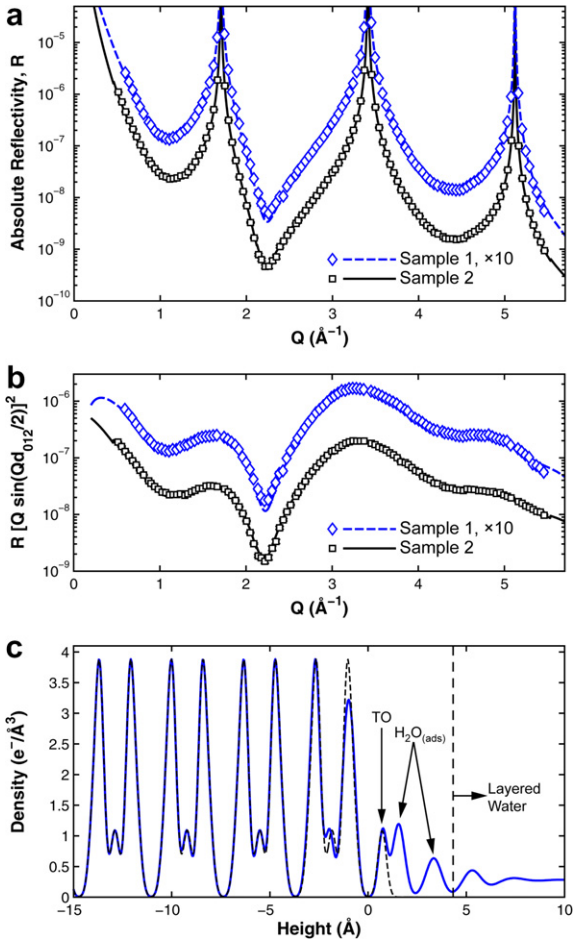

Fig. 2. Least-squares fitting results: (a) absolute reflectivity data (symbols) and the reflectivity calculated for the best-fit model (lines); (b) normalized reflectivity data (symbols) and fits (lines); and (c) electron density profiles of the initial bulk termination (dashed) and the full refined structure (solid) of the hematite (0 1 2)–water interface. Statistical errors in the data are not visible as they are smaller than the symbol sizes.

Table 1
Optimized structural parameters from best-fit model of the α-Fe_2O_3 (0 1 2)–water interface

Surface structure				
Atom	z_{init} (Å)[a]	z (Å)[b]	σ (Å)[c]	θ[d]
O (H_2O_{ads})[e]		3.3(3)[f]	0.3(2)	1.1(4)
O (H_2O_{ads})		1.6(2)	0.2(2)	1.6(6)
O (>FeO)	0.716	0.7(1)	0.071	1
O (>Fe_3O)	−0.716	−0.7(3)	0.071	1
Fe	−1.066	−1.07(7)	0.2(1)	1
O	−1.841	−2.0(1)	0.071	1
Fe	−2.617	−2.65(6)	0.064	1
O	−2.967	−3.00(6)	0.071	1
O	−4.399	−4.41(3)	0.071	1
Fe	−4.748	−4.76(3)	0.064	1
O	−5.524	−5.5(1)	0.071	1
Fe	−6.300	−6.30(1)	0.064	1
O	−6.649	−6.65(1)	0.071	1
O	−8.081	−8.088(6)	0.071	1
Fe	−8.431	−8.438(6)	0.064	1
O	−9.207	−9.23(2)	0.071	1
Fe	−9.982	−9.985(4)	0.064	1
O	−10.332	−10.335(4)	0.071	1

Layered water structure			
z (Å)	σ_o (Å)	$\bar{\sigma}$ (Å)	d_w (Å)
5.3(3)	0.4(1)	0.4(2)	1.9(2)

Sample-specific non-structural parameters		
Sample	Water film (μm)	Roughness (Å)
1	30(20)	2(1)
2	0(40)	2(1)

For a detailed description of the fitting parameters see Catalano et al. (2006b).

[a] Atom height for the unrelaxed (bulk) structure.

[b] Atom height from the best-fit model.

[c] Vibrational amplitude.

[d] Occupancy per 13.66 Å^2, half of a surface unit cell.

[e] Near-surface oxygen sites are labeled assuming a half-layer termination.

[f] Uncertainties in the last digit are listed in parentheses, reported at the 95% confidence level. Parameters with no listed uncertainties were not varied in the analysis.

ways within error of full occupancy (e.g., 0.95 ± 0.15), and the occupancy was thus fixed to 1 in the final structural refinement. The occupancies of O sites similarly refined to within error of full occupancy during preliminary fitting, although the errors were larger than those seen for the Fe site because of the weaker contribution of O to the total X-ray scattering from the surface.

This structural model also included ordered water components above the hematite surface. Two sites of "adsorbed" water were included, similar to those seen on the corundum (0 1 2) surface in a past study (Catalano et al., 2006b). The lower of the two sites had a smaller vibrational amplitude and a nominally higher occupancy, although the occupancies of both sites were not statistically different from that of the oxygen sites in the bulk structure. A layered bulk water profile, with ordering that decays away from the hematite surface, fit the data better than a featureless bulk water profile ($\chi^2 = 7.55$ for featureless water).

The extrinsic parameters were generally consistent with those seen in past studies of surface structures (Trainor et al., 2002, 2004; Park et al., 2004; Catalano et al., 2006b; Tanwar et al., 2007a,b). Sample-specific surface roughness converged to statistically identical values for the two samples, further supporting the reproducibility of the sample preparation. Water film thicknesses differed for the two samples, but were within error. The data for sample 2 were collected using an X-ray energy that experiences little attenuation by a thin water film. Thus, measurements on sample 2 are insensitive to the water (and plastic) film covering the surface, and the resulting water film thickness value has poor precision.

Goodness-of-fit parameters (χ^2) reported in many past studies of hydrated hematite and corundum surface structures are often much smaller (Table 2) than that determined for the best-fit model in this study (5.17). At first glance this would seem to suggest that the models reported in those

Table 2
Comparison of χ^2 values determined in past X-ray scattering studies of the structure of hydrated hematite and corundum surfaces

Surface	χ^2	Reference
Corundum (0 0 1)	1.37	Eng et al. (2000)
Corundum (0 1 2)[a]	1.6	Trainor et al. (2002)
Corundum (0 1 2)[a]	2.23	Catalano et al. (2006b)
Hematite (0 0 1)	1.91	Trainor et al. (2004)
Hematite (0 1 2)[a]	3.8	Tanwar et al. (2007a)
Hematite (0 1 2)[b]	1.2	Tanwar et al. (2007b)
Hematite (0 1 2)[b]	5.17	This study

[a] Structure of the half-layer termination.
[b] Structure of the full-layer termination.

studies better reproduced the data (and are thus more accurate) than the model proposed in the current work. However, χ^2 is not, by itself, sufficient for comparing fits in different studies, as it is dependent not only on the difference between the calculated and measured data, but also the uncertainties in the data (see Eq. (1)). The data presented in this study have experimental precisions at least four times smaller than those in past studies of hydrated hematite and corundum surfaces, with the exception of the most recent study of the corundum (0 1 2)–water interface by Catalano et al. (2006b). To put this in perspective, if the experimental uncertainties in the current study were uniformly four times larger, then the χ^2 value would decrease by a factor of 16 (from 5.17 to 0.32). Thus, the χ^2 value reported in this study indicates that our model reproduces the data significantly better than the models presented in past studies when we account for the differences in experimental uncertainties of individual measurements. The high degree of agreement between our data and the best-fit model over a range of four orders of magnitude is indicated by the *R*-factor for the best-fit model, indicating an average deviation of only ~4.5%, which is a similar magnitude to the level of systematic error that we saw in repeated fiducial measurements.

3.2. Interfacial structure

The observation of only minor relaxations of the hematite structure near the surface demonstrates that the stability of the bulk structure is affected little by the creation of a surface. This stability is likely the result of the general stability of Fe(III) octahedra. The resulting surface structure preserves charge balance, excluding changes from surface functional group protonation and deprotonation, while creating a stable coordination geometry for the near surface iron atoms. The most substantial relaxations are localized at the hematite–water interface, suggesting surface effects on the structure are limited to the top most atomic layers. This limited relaxation of the structure has been seen for multiple oxide and silicate minerals surface (Eng et al., 2000; Fenter et al., 2000, 2003; Schlegel et al., 2002; Trainor et al., 2002, 2004; Fenter and Sturchio, 2004; Catalano et al., 2006b; Tanwar et al., 2007a,b).

The well-defined vertical positions of the two adsorbed water sites with respect to the hematite surface normal suggest that these water molecules occupy specific locations above the surface, and are thus specifically adsorbed. While the lateral position of each feature at the interface could not be determined as these specular XR data are only sensitive to their location normal to the surface, we can infer their

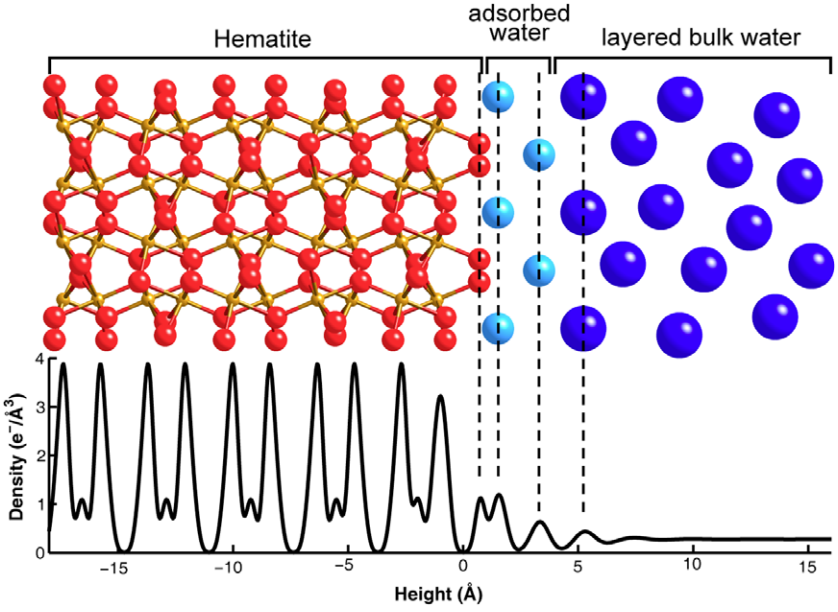

Fig. 3. Structural model of hematite (0 1 2)–water interface viewed from [1 2 $\bar{1}$] in relation to the electron density profile. The small spheres in the hematite structure are Fe and the large spheres are O. H atoms were not included in the model as their positions cannot be determined by X-ray reflectivity. Note that the lateral positions of the adsorbed water molecules have not been determined experimentally, only being inferred from steric constraints.

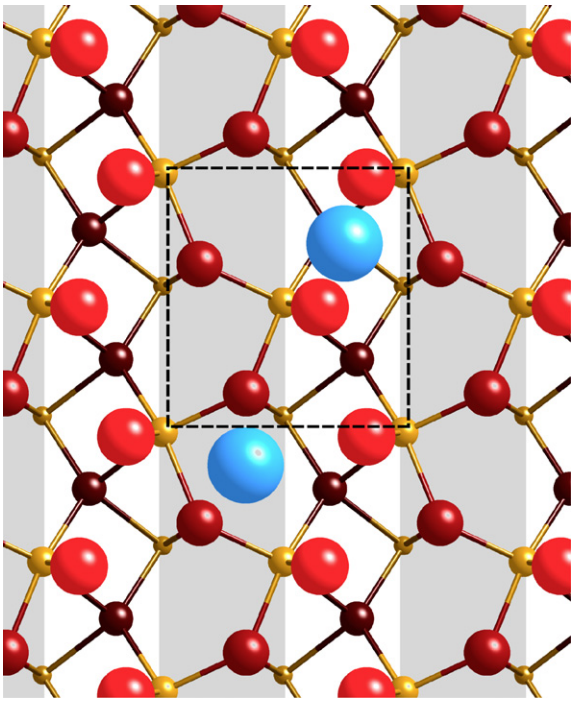

Fig. 4. Top view of the hematite (0 1 2) surface showing the hypothesized lateral ordering of adsorbed water (large sphere). The shaded areas are the valley regions on the hematite surface.

approximate lateral location from the measured interfacial structure and by applying reasonable structural constraints. The hematite (0 1 2) surface is corrugated with alternating ridges of singly coordinated oxygen groups and valleys over triply coordinated oxygen groups running parallel to $[1\,2\,\bar{1}]$. The lower adsorbed water site must be laterally located in these valleys (Fig. 3), as it would otherwise overlap with the singly coordinated oxygen site, which is not sterically feasible. The height of this water site also suggests that it occupies a specific site bridging between two adjacent triply coordinated oxygen groups in these valleys (Fig. 4), as only this geometry produces O–O interatomic distances $\geqslant 2.7$ Å, assuming the surface atoms are at the heights determined experimentally and in their bulk positions laterally. Considering the uncertainties in the heights of the near-surface oxygen atoms (Table 1), and the generally small lateral relaxations seen in studies of hydrated metal oxides surfaces (Eng et al., 2000; Trainor et al., 2004; Tanwar et al., 2007a,b), the interatomic distances for this site are close to ideal for a water molecule that is hydrogen bonded to nearby surface functional groups and other interfacial water molecules.

The upper adsorbed water molecules also may also be laterally ordered. The molecules in the upper site appear to be located above the ridges of singly coordinated oxygen groups in order to obtain realistic interatomic distances with the lower adsorbed water site in the valleys on the hematite (0 1 2) surface. Above these ridges, the upper adsorbed water molecules would maintain 2.95–3.00 Å O–O interatomic distances with the singly coordinated functional groups if they took on a bridging geometry. This geometry would also maintain a separation between two adjacent adsorbed water molecules (one upper, one lower) of ~2.85 Å.

The locations of adsorbed water, as inferred from the XR-derived heights and steric constraints, suggests that the hematite (0 1 2) surface serves as a template for the ordering of water in the interfacial region. The resulting arrangement of water molecules minimizes the unoccupied space above the surface and acts as a bridge between the ordered mineral structure and disordered bulk water. The layered water profile included in the best-fit structural model likely represents a continuation of this structural bridging, as the adsorbed water will serve to further template the structure of interfacial water but with gradually reducing positional order with respect to the mineral substrate. The decaying order observed in this study likely reflects the soft structure and dynamic bonding behavior of water.

3.3. Comparison to previous studies of hematite (0 1 2) interfacial structure

Two recent experimental studies have examined the structure of hydrated hematite (0 1 2) surfaces having predominantly a half-layer (Tanwar et al., 2007a) and full-layer (Tanwar et al., 2007b) termination [for a discussion and explanation of these two terminations, see recent work by Catalano et al., 2006b, 2007 and Tanwar et al., 2007a,b]. Both studies measured the specular XR as well as multiple non-specular crystal truncation rods, although the data were of uniformly lower precision than the data reported in the current work. In addition, both studies made their measurements in the presence of humidified He gas, not under water or aqueous solution.

The study of Tanwar et al. (2007b) examined a sample prepared similarly to the samples examined in this study that nominally displayed the same termination, and is thus most relevant for comparison. It should be noted that the Tanwar et al. (2007b) study was focused on examining the dependence of termination on surface preparation, and did not seek to obtain as detailed a structural refinement as presented in Tanwar et al. (2007a) or in the present work. As done here, Tanwar et al. (2007b) refined a starting structural model based on a full-layer termination of the hematite (0 1 2) surface. However, in that study only the top Fe_2O_3 layer was allowed to relax (plus a terminal oxygen site that completes the upper Fe coordination shell), all vibrational amplitudes (as isotropic Debye–Waller factors) were fixed, and no adsorbed or layered water was included in the model; the atomic positions were refined in three dimensions as both specular and non-specular reflectivity data were collected. Differences in the relaxed vertical positions of most near-surface atoms between the two studies were within the least-squares fitting errors ($\pm 2\sigma$), with the exception of the singly coordinated oxygen site. The unrelaxed, bulk height of this site is 0.72 Å (from the origin used in this study); the fitting results presented here located this site at a height of 0.7 ± 0.1 Å, while Tanwar et al. (2007b) reported the singly coordinated oxygen at 0.88 ± 0.05 Å. We suspect that the Tanwar et al.

(2007b) height for this site may be less accurate as adsorbed water sites were not included in the structural model in the study. Adsorbed water has been seen in multiple past X-ray scattering studies of metal oxides surfaces measured in a humidified gas environment (Eng et al., 2000; Trainor et al., 2004; Tanwar et al., 2007a), and the direct inversion results presented above clearly show two adsorbed water sites for the samples examined under water in the present study.

A larger difference between the two studies is seen when comparing the occupancies of the atom sites in the top Fe_2O_3 layer. These are all fully occupied in the refined structural model in this study, while many are less than 1, though no smaller than 0.7, in the Tanwar et al. (2007b) study. As noted above, attempts to refine site occupancies in the present study always led to results well within error of full occupancy. This discrepancy in site occupancies may reflect the differences in the level of detail of the structure refinements, as the Tanwar et al. (2007b) study only refined the positions of the top Fe_2O_3 layer and did not include sites of adsorbed water. Alternatively, allowing the occupancies of all the atoms in the top Fe_2O_3 layer to vary may have produced an unintended correlation with the roughness parameter that resulted in all occupancies refining to less than 1 in that study. A reduction of all the occupancies in a layer produces an effect on the scattering similar to the roughness model of Robinson (1986) but with a different functional form, although the effects are qualitatively very similar. Thus, the reduced occupancies in Tanwar et al. (2007b) may actually be simulating part of the surface roughness instead of representing true structural details associated with a mixture of terminations or intrinsic vacancies near the mineral surface. Finally, it is possible that the crystal studied in Tanwar et al. (2007b) was not annealed long enough to reach full occupancy of the upper Fe site; additional measurements of the dependence of the hematite (0 1 2) surface structure on annealing time and temperature are needed to evaluate this possibility.

One previous study has examined the location of adsorbed water sites on a hematite (0 1 2) surface (Tanwar et al., 2007a), but direct comparison of the arrangement of adsorbed water proposed here with the positions suggest in this previous study is not possible as the surface termination differed in the two studies. Qualitatively, both studies observed the presence of adsorbed water at two different heights above the surface. However, the Tanwar et al. (2007a) study found that the lower water site was above the terminal oxygen row on the half-layer termination, whereas in the present work we suggest a similar site is located above the valleys on the full-layer termination (see discussion in Section 3.2). As the lateral adsorbed water positions in the Tanwar et al. (2007a) study differ from those proposed by Lo et al. (2007) in a computation study of that termination, as the sites proposed by Tanwar et al. (2007a) produce O–O distances between adsorbed water and surface functional groups as short as 2.0 ± 0.3 Å, too short to be sterically feasible, and as the lateral positions of adsorbed water sites were not determined in the present work, future study is needed to determine the true lateral arrangement of adsorbed water on hematite (0 1 2) surfaces.

3.4. Comparison of hematite and corundum (0 1 2) interfacial structures

Hematite and corundum are isostructural phases, only differing in lattice parameters and the cation type. Although the (0 1 2) surfaces of these phases can display two different, inequivalent terminations as well as a mixture of the two (Catalano et al., 2006b, 2007; Tanwar et al., 2007a,b), the ability to control which of these two terminations a specific sample exhibits has been established through details of the sample preparation (Tanwar et al., 2007b). In this and an earlier study (Catalano et al., 2006b), the interfacial structure of corundum and hematite (0 1 2) surfaces were found to have the same termination. This allows a direct comparison of the relaxations in the near-surface layers of the mineral lattice as well as their affects on the interfacial water structure.

3.4.1. Mineral surface relaxations

The relaxations of both the hematite and corundum (0 1 2) surface are primarily limited to the top layer of the mineral structure (Fig. 5). The second and third layers below the surface display relaxations of generally 0.02 Å or less. Relaxation in the top layer are primarily localized on the upper half of this layer, with a general broadening of the density feature that results from the upper Fe and triply coordinated O sites. In the analysis of the hematite structure this broadening was modeled as an increased vibrational amplitude of the upper Fe site. In the corundum analysis, this was associated with an outward shift of the triply coordinated O site. Attempts were made to refine the vibrational amplitude of the upper Al site in the corundum structure, but this parameter correlated with the height of the triply coordinated O site, and was fixed at its bulk value (Catalano et al., 2006b). Based on the hematite results it is likely that the upper Al site in corundum also had a vibrational amplitude larger than the bulk value. Because of the resolution of the data and small difference in electron density of Al and O, an outward shift in the triply coordi-

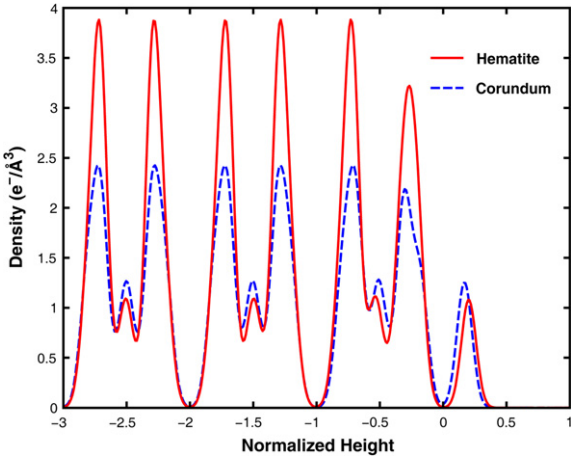

Fig. 5. Comparative relaxations of the hematite and corundum (0 1 2) surfaces. Height has been normalized to the thickness of one Fe_2O_3/Al_2O_3 layer.

nated O site and an increased vibrational amplitude of Al have a similar effect on the total density profile, and are thus difficult to distinguish. In the case of hematite, an outward shift of the O site does not produce the same density effect as an increased vibrational amplitude of Fe because of the large difference in electron density between Fe and O; thus, both the O position and the Fe vibrational amplitude were able to be refined together.

The limited relaxations seen on the corundum and hematite (0 1 2) surfaces are consistent with the past observation that most surfaces of minerals in contact with water having structures containing stable polyhedral units, like metal oxides and silicates, generally display minor surface relaxations and rarely reconstruct (Fenter and Sturchio, 2004). In fact, reconstructions previously seen on iron and aluminum oxides (e.g., Hsu and Kim, 1991a,b; Gautier-Soyer et al., 1996; Henderson et al., 1998, 2002) only occur in ultra high vacuum (UHV) environments after the formation of oxygen vacancies on the surface, a process unlikely to take place in aqueous solution. Thus, the surfaces of iron and aluminum oxide phases under conditions where chemical species (e.g., water) are available to maintain a stable coordination (i.e., octahedral) of Fe and Al will likely always display only minor changes in the metal–oxygen bond lengths and arrangements of surface functional groups predicted from the bulk structure. This would suggest that assuming a bulk-like arrangement of surface functional groups positions is a good first approximation when evaluating the potential reactivity of metal oxide surfaces.

3.4.2. Water ordering and structure

The arrangement of water is also similar at the hematite and corundum (0 1 2)–water interfaces (Fig. 6). Both surfaces display two sites of adsorbed water at similar heights above the surface as well as layering that extends about 1 nm into solution. However, ordering of interfacial water decays faster from the surface on hematite, with only the first adsorbed water site having a similar vibrational amplitude as seen on corundum. One possible explanation for the differences in water ordering between these surfaces may be the differences in O–O distances between the corundum and hematite lattices. Corundum displays O–O distance of 2.52–2.86 Å, with an average distance of 2.72 Å (Ishizawa et al., 1980), whereas hematite displays O–O distances of 2.66–3.03 Å, with an average distance of 2.88 Å (Finger and Hazen, 1980). Recent X-ray scattering studies of liquid water structure display a maximum in the O–O pair correlation function at 2.73 Å (Hura et al., 2000; Sorenson et al., 2000), similar to the average O–O spacing in corundum. This suggests that the oxygen lattice, and thus the surface functional group arrangement, of corundum may better match the natural structuring of water than that of hematite, and thus may induce stronger ordering of the interfacial water.

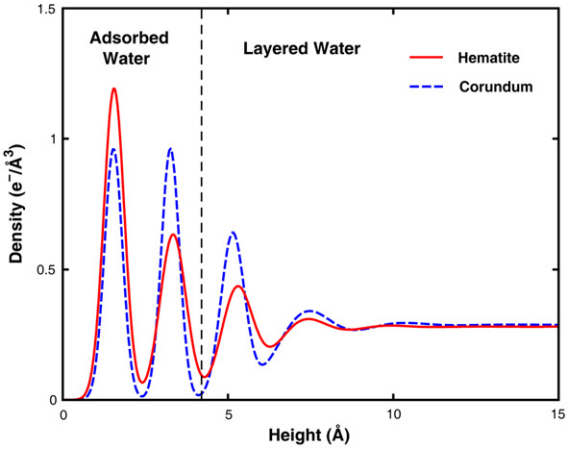

Fig. 6. Comparison of water structures on the hematite and corundum (0 1 2) surfaces.

Alternatively, surface functional group exchange dynamics may play a role in determining interfacial water ordering. We are unaware of measurements of water exchange rates on surfaces of iron and aluminum oxide phases, and none have been made on the specific surfaces discussed in this study, but such rates can be estimated through analogy with those measured on aluminum and iron solution species and aluminum oxide and molybdenum–iron oxide molecular clusters. Water exchange rates of η-OH_2 groups (comparable to singly coordinated functional groups on mineral surfaces) are ~2 orders of magnitude faster for $Fe(OH_2)_6^{3+}$ than $Al(OH_2)_6^{3+}$ and ~1 order of magnitude faster for $Fe(OH_2)_5OH^{2+}$ than $Al(OH_2)_5OH^{2+}$ (Grant and Jordan, 1981; Hugi-Cleary et al., 1985; Nordin et al., 1998). The exchange rates of η-OH_2 group on various aluminum polyoxocations and solution monomers fall into a small range 2–4 orders of magnitude faster than that of $Al(OH_2)_6^{3+}$ (Casey et al., 2000; Phillips et al., 2000, 2003; Casey and Phillips, 2001). Although such exchange rates on comparable Fe(III) species have not been measured, exchange rates of Fe–OH_2 groups on Keplerate Mo–Fe solution clusters and Fe(III) complexed by EDTA and its derivatives (Schneppensieper et al., 2001; Balogh et al., 2007) are between 2 and 6 orders of magnitude faster than the Al–OH_2 exchange rates of the solution species and clusters discussed above. Taken together, this suggests that water exchange rates of Fe(III) species are uniformly faster than for comparable Al(III) species, and it is reasonable to assume that singly coordinated oxygen functional groups on hematite will have faster exchange rates than on corundum. It is thus possible that the weaker ordering of water seen near the hematite surface may be partly due to this suspected difference in exchange dynamics.

The differences in the strength of ordering of interfacial water on hematite and corundum (0 1 2) suggest that the gradients in the interfacial dielectric constants of water in the near-surface regions may differ as well. Although thought to be less than that of bulk water, and lower for the first water layer above a surface than for the second, the dielectric constant of interfacial water has not been measured accurately because it is difficult to access experimentally (Brown et al., 1999). An approximate interfacial dielectric constant of 53 (dielectric constant of bulk water is 78) was suggested for both hematite and corundum (Sverjensky, 2001). The present results suggest that these two materials likely have different gradients in the interfacial

dielectric constants, although these differences may be small. The assumption of equivalent dielectric constants may be an acceptable first approximation for surface complexation modeling. It should be noted that other hematite and corundum surface may show different interfacial dielectric constants, as the distribution of surface functional groups and degree of atomic-scale topography, which may produce a near-surface charge distribution that varies substantially but periodically across the surface, are orientation-specific.

3.5. Comparative surface chemistry of hematite and corundum (0 1 2)

Ignoring the obvious differences in redox chemistry, the reactivity of iron and aluminum oxide surfaces towards aqueous chemical species is dependent on the type and arrangement of surface functional groups exposed. As both the hematite and corundum (0 1 2) surfaces display isostructural terminations, their distribution of surface functional groups is the same, although hematite has fewer sites per unit area because of its larger lattice parameters. The pK_a of surface functional groups, and thus the charging behavior, of the two surfaces are expected to be similar as well (within ~1 pH unit). pK_a values are often predicted based on bond valence parameters (Hiemstra et al., 1989, 1996), which are nominally the same for similar types of surface functional groups on the two surfaces. Slight differences in pK_a values are expected because of differences in Fe–O and Al–O bond length asymmetry (i.e., cation octahedra are distorted in corundum-type structures) and surface relaxations.

Hematite and corundum (0 1 2) surfaces are also expected to display generally similar reactivity towards adsorbates. Recent studies of arsenate adsorption on these surfaces highlight these similarities. Arsenate reacts with hematite and corundum (0 1 2) surfaces to form both bridging-bidentate inner-sphere surfaces complexes as well as non-bonded outer-sphere complexes (Catalano et al., 2006c). The ratio of inner-sphere to outer-sphere complexes was higher on hematite, indicating subtle differences in reactivity, but the general uptake behavior and adsorption mechanisms were the same on both surfaces. Differences in the ordering of interfacial water discussed above may be the cause of the higher inner-sphere to outer-sphere ratio on hematite. Further study is needed to verify that corundum and hematite (0 1 2) surfaces display similar reactivity towards other adsorbates.

4. CONCLUSIONS

XR measurements of the hematite (0 1 2)–water interface demonstrate that relaxations are localized to the top most atomic layers of the structure and that interfacial water orders, likely through hydrogen bonding to surface functional groups. Hematite and corundum (0 1 2) display similar surface relaxations, and similarities in the arrangement of water at the hematite and corundum (0 1 2) surfaces reflect the isostructural distributions of surface functional groups. The ordering of interfacial water decayed more rapidly away from the surface at the hematite–water interface, which we suggest might be due to the apparent better match of the corundum oxygen lattice with the natural ordering of water or the expected faster exchange rates of hematite surface functional groups with water. Although previously suggested to have the same interfacial dielectric constants (Sverjensky, 2001), the weaker ordering at the hematite surface suggests that the interfacial dielectric constant gradient may be larger here than at the corundum surface. The similar distribution of surface functional group types on hematite and corundum (0 1 2) surfaces suggest that these surfaces display similar charging behavior and may have similar reactivity towards adsorbates. Recent studies of arsenate adsorption support this hypothesis but also demonstrate subtle differences in reactivity that may be related to the observed differences in interfacial water ordering.

ACKNOWLEDGMENTS

This work was supported by the Argonne National Laboratory Named Postdoctoral Fellowship Program and the Geosciences Research Program of the Office of Basic Energy Sciences, US Department of Energy (DOE), through contract DE-AC02-06CH11357. The data were collected at the X-ray Operations and Research (XOR) beamlines 20-ID-C (PNC/XOR) and 11-ID-D (BESSRC/XOR) at the Advanced Photon Source (APS), Argonne National Laboratory. PNC/XOR facilities, and research at these facilities, are supported by the US Department of Energy—Basic Energy Sciences, a major facilities access grant from NSERC, the University of Washington, Simon Fraser University, the Pacific Northwest National Laboratory and the Advanced Photon Source. Use of the Advanced Photon Source is also supported by the US Department of Energy, Office of Science, Office of Basic Energy Sciences, under Contract DE-AC02-06CH11357. Julie Cross, Steve Heald, and Klaus Attenkofer are thanked for their help with beamline operations, and Zhang Zhang and Vaibhav Kohli are thanked for their assistance during data collection. Comments from the Associate Editor (Bill Casey), Tom Trainor, and two anonymous referees are also appreciated.

APPENDIX A. X-RAY REFLECTIVITY FROM AN IDEALLY MISCUT SURFACE

Polished surfaces are often 'miscut' (Andrews and Cowley, 1985; Pflanz et al., 1995; Munkholm and Brennan, 1999), that is, the orientation of the crystallographic planes is misaligned by an angle, α, with respect to the physical surface plane (see Fig. A1a). At the molecular level, this can result in a surface with regularly stepped terraces, with a step spacing $L_{step} = Ma = c/\sin(\alpha)$, where M is the number of unit cells separating each step, a is the lattice spacing perpendicular to the step, and c is the vertical lattice spacing. Crystal truncation rods (CTRs) are oriented normal to the physical surface (Fig. A1b). CTRs from an ideally miscut surface are therefore tilted and segmented, emanating from each of the substrate lattice Bragg peaks. For the measurements described in this manuscript, two of the rods were measured at each q_z value. Here we describe the impact of this on the quantification of the measured intensities.

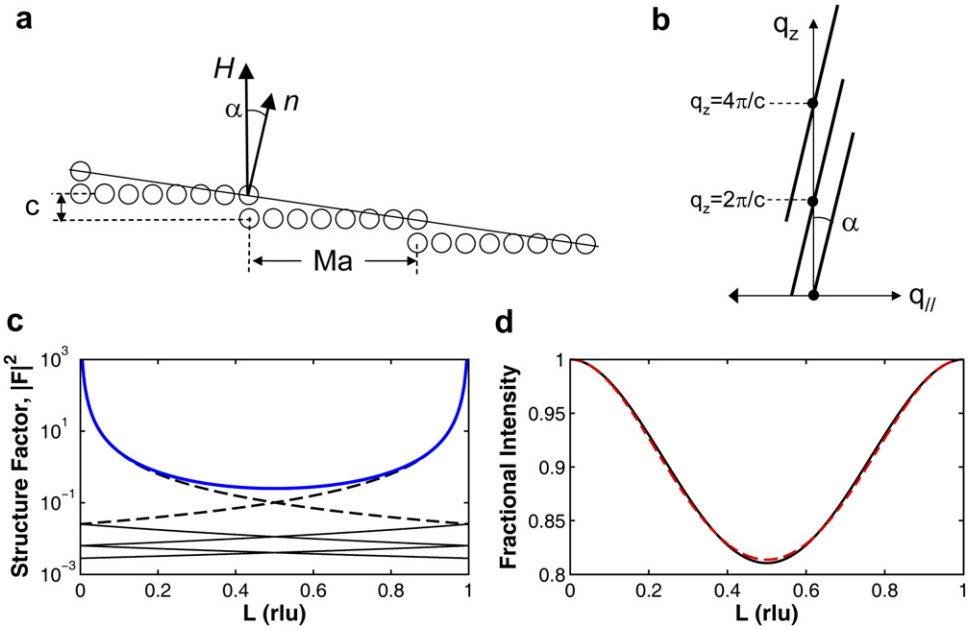

Fig. A1. (a) Schematic of a miscut surface with a terrace size Ma and a vertical layer spacing c. Here the surface normal, n, is tilted by an angle, $\alpha = c/Ma$, with respect to the crystallographic direction H. (b) Schematic of the reciprocal space structure of a miscut surface as a function of the vertical and lateral momentum transfers, q_z and $q_{//}$, respectively. The CTRs for a miscut surface emanate from the bulk Bragg peak locations (e.g., $q_z = 2\pi/c$) and are also tilted by the same angle, α, with respect to the bulk Bragg peak. (c) Structure factor magnitude as a function of vertical momentum transfer (shown here in reciprocal lattice units L, where $q_z = L(2\pi/c)$, where $L = 1, 2, 3$ are the Bragg peak locations). The bold line indicates the structure factor of a flat surface, the other lines indicate the q_z-variation of the miscut CTRs with the rods emanating from $L = 0$ and 1 shown as dashed lines. (d) The fraction of the intrinsic reflectivity measured with the two strongest miscut rods, as a function of vertical reciprocal units (solid line). Also shown is the roughness factor for calculated for $\beta = 0.052$ (dashed line).

As described previously, the specular reflectivity of a miscut surface can be expressed as an interfacial structure factor in which all of the atoms within each terrace are explicitly included (Munkholm and Brennan, 1999). This can be written as:

$$F = F_{\text{flat}} F_{\text{terrace}} F_{2\text{d}}$$

where $F_{\text{flat}} = F_{\text{UC}} F_{\text{CTR}} + F_{\text{surf}}$ is the intrinsic structure factor of the ideally oriented surface (including the substrate unit cell crystal structure, F_{UC}, the semi-infinite layering of the crystal below the surface, F_{CTR}, and the interfacial structural displacements as well as interfacial water structure, F_{surf}). F_{terrace} is the structure factor of the M unit cells that define each terrace, and $F_{2\text{d}}$ is the infinite sum over all terraces across the surface

$$F_{2\text{d}} = \delta([q_z c - q_{//} Ma]/2 - H\pi) \tag{A.1}$$

$$F_{\text{terrace}} = (1/M)\sin(Mq_{//}a/2)/\sin(q_{//}a/2) = \sin\{[q_z - q_z^0]c/2\}/\{[q_z - q_z^0]c/2\} \tag{A.2}$$

where, q_z and $q_{//}$ are the vertical and lateral momentum transfers with respect to the flat terraces, H is any integer, and q_z^0 is the vertical momentum transfer of any substrate Bragg reflection (we have suppressed phase factors that do not contributed to the measured intensities). From Eq. (A.1), we see that $q_{//} = [q_z - q_z^0]c/Ma$ where H is an integer. This relationship between $q_{//}$ and q_z reveals that the crystal truncation rod is tilted by an angle, α, defined by the relation: $c/Ma = \sin(\alpha)$. That is, the CTR remains perpendicular to the physical surface. This expression also shows that the CTR extends from each of the bulk Bragg peak locations and that the terrace structure factor is an interference function that is peaked at a single substrate Bragg peak, q_z^0. The expression for F_{terrace} is evaluated on a per unit cell basis (Eq. (A.2)) making only two assumptions: that each unit cell in the terrace is identical (i.e., ignoring differences in structural displacements across each terrace) and that $[q_z - q_z^0]c/2M \ll 1$, or equivalently, $\Delta L \ll M$, where $\Delta L = (q_z - q_z^0)c/2\pi$. These conditions are easily satisfied for the present measurements with $M \sim 100$.

In the present measurements, typically only the two strongest miscut rods at each q_z were measured. Consequently reflected intensity is missing from the measurements associated with the unmeasured rods. The structure factor for these two rods (e.g., emanating from $q_z = 0$ and $2\pi/c$; dashed lines Fig. A1c) is compared with that from a flat surface in (bold blue line, Fig. A1c), as well as other unmeasured rods emanating from $q_z = -2\pi/c$, $4\pi/c$, etc, (solid black lines Fig. A1c) to evaluate the significance of this experimental detail. We also plot the sum of the two strongest miscut rods divided by that calculated for the ideally flat surface (Fig. A1d). From this we see that ~20% of the intrinsic reflectivity is missing from the sum of the two strongest miscut rods near the mid-zones of the CTR, but that the intrinsic structure factor is obtained near the Bragg peak locations. This far exceeds the ~1–2% statistical uncertainty of the experimental data and therefore must be included

explicitly in the analysis. The q_z-variation of this missing intensity mimics that of an atomically rough surface (Robinson, 1986), described by the parameter $\beta = 0.052$, corresponding to an effective rms roughness of $\sim c/4$, and is independent of the magnitude of the miscut angle (within the assumptions described above in deriving Eqs. (A.1) and (A.2)). That is, ignoring the details of which miscut rods were measured would result in a mistaken interpretation that the surface is intrinsically rough. To avoid this systematic error, the specular reflectivity that is compared to the data in the model fits is calculated for the specific miscut rods that were measured, each indexed by the vertical momentum transfer, q_z, and the Bragg peak from which it emanates, q_z^i. That is, $R(q_z, q_z^i) = R_{\text{flat}}(q_z)|^2 \Sigma_i \mid F_{\text{terrace}}(q_z, q_z^i)|^2$. In this way, the structure factor calculations are done for the specific measurements that were performed. Because the relative intensity of the miscut rods is determined by $\mid F_{\text{terrace}}(q_z, q_z^i) \mid$, which does not depend on the details of the interfacial structure or on the precise miscut angle, measurement of any individual miscut CTR at a given q_z is sufficient for comparison to the structural models. In some cases, the measured and calculated CTR intensities may appear to have discontinuities as a function of q_z. This is an artifact of terminating the integration of a CTR before its intensity decayed to a negligible value.

REFERENCES

Al-Abadleh H. A. and Grassian V. H. (2003) Oxide surfaces as environmental interfaces. *Surf. Sci. Rep.* **52**, 63–161.

Andrews S. R. and Cowley R. A. (1985) Scattering of X-rays from crystal surfaces. *J. Phys. C: Solid State Phys.* **18**, 6427–6439.

Balogh E., Todea A. M., Muller A. and Casey W. H. (2007) Rates of ligand exchange between $>Fe^{III}$-OH_2 functional groups on a nanometer-sized aqueous cluster and bulk solution. *Inorg. Chem.* **46**, 7087–7092.

Bargar J. R., Trainor T. P., Fitts J. P., Chambers S. A. and Brown, Jr., G. E. (2004) In situ grazing-incidence extended X-ray absorption fine structure study of Pb(II) chemisorption on hematite (0001) and $1\bar{1}02$ surfaces. *Langmuir* **20**, 1667–1673.

Brown, Jr., G. E., Henrich V. E., Casey W. H., Clark D. L., Eggleston C., Felmy A., Goodman D. W., Gratzel M., Maciel G., McCarthy M. I., Nealson K. H., Sverjensky D. A., Toney M. F. and Zachara J. M. (1999) Metal oxide surfaces and their interactions with aqueous solutions and microbial organisms. *Chem. Rev.* **99**, 77–174.

Brown, Jr., G. E. (2001) How minerals react with water. *Science* **294**, 67–70.

Casey W. H. and Phillips B. L. (2001) Kinetics of oxygen exchange between sites in the $GaO_4Al_{12}(OH)_{24}(H_2O)_{12}{}^{7+}$(aq) molecule and aqueous solution. *Geochim. Cosmochim. Acta* **65**, 705–714.

Casey W. H., Phillips B. L., Karlsson M., Nordin S., Nordin J. P., Sullivan D. J. and Neugebauer-Crawford S. (2000) Rates and mechanisms of oxygen exchanges between sites in the $AlO_4Al_{12}(OH)_{24}(H_2O)_{12}{}^{7+}$(aq) complex and water: Implications for mineral surface chemistry. *Geochim. Cosmochim. Acta* **64**, 2951–2964.

Catalano J. G., Trainor T. P., Eng P. J., Waychunas G. A. and Brown, Jr., G. E. (2005) CTR diffraction and grazing-incidence EXAFS study of U(VI) adsorption onto α-Al_2O_3 and α-Fe_2O_3 ($1\bar{1}02$) surfaces. *Geochim. Cosmochim. Acta* **69**, 3555–3572.

Catalano J. G., Zhang Z., Fenter P. and Bedzyk M. J. (2006a) Inner-sphere adsorption geometry of Se(IV) at the hematite (100)–water interface. *J. Colloid Interface Sci.* **297**, 665–671.

Catalano J. G., Park C., Zhang Z. and Fenter P. (2006b) Termination and water adsorption at the α-Al_2O_3 (012)—aqueous solution interface. *Langmuir* **22**, 4668–4673.

Catalano J. G., Park C., Zhang Z. and Fenter P. (2006c) Simultaneous inner- and outer-sphere arsenate adsorption on iron and aluminium oxide surfaces. *Geol. Soc. Am. Abstr. Programs* **38**(7), 242.

Catalano J. G., Zhang Z., Park C., Fenter P. and Bedzyk M. J. (2007) Bridging arsenate surface complexes on the hematite (012) surface. *Geochim. Cosmochim. Acta* **71**, 1883–1897.

Cromer D. T. and Liberman D. (1970) Relativistic calculation of anomalous scattering factors for X-rays. *J. Chem. Phys.* **53**, 1891–1898.

Davis J. A. and Kent D. B. (1990) Surface complexation modeling in aqueous geochemistry. *Rev. Miner.* **23**, 177–260.

Eng P. J., Trainor T. P., Brown, Jr., G. E., Waychunas G. A., Newville M., Sutton S. R. and Rivers M. L. (2000) Structure of the hydrated α-Al_2O_3 (0001) surface. *Science* **288**, 1029–1033.

Fenter P. (2002) X-ray reflectivity as a probe of mineral–fluid interfaces: a user guide. *Rev. Miner. Geochem.* **49**, 149–220.

Fenter P. and Park C. (2004) Termination interference along crystal truncation rods of layered crystals. *J. Appl. Crystallogr.* **37**, 977–987.

Fenter P. and Sturchio N. C. (2004) Mineral–water interfacial structures revealed by synchrotron X-ray scattering. *Prog. Surf. Sci.* **77**, 171–258.

Fenter P. and Zhang Z. (2005) Model-independent one-dimensional imaging of interfacial structures at <1 Å resolution. *Phys. Rev. B* **72**, 081401.

Fenter P., Teng H., Geissbuhler P., Hanchar J. M., Nagy K. L. and Sturchio N. C. (2000) Atomic-scale structure of the orthoclase (001)–water interface measured with high-resolution X-ray reflectivity. *Geochim. Cosmochim. Acta* **64**, 3663–3673.

Fenter P., Cheng L., Park C., Zhang Z. and Sturchio N. C. (2003) Structure of the orthoclase (001)– and (010)–water interfaces by high-resolution X-ray reflectivity. *Geochim. Cosmochim. Acta* **67**, 4267–4275.

Fenter P., Catalano J. G., Park C. and Zhang Z. (2006) On the use of CCD area detectors for high-resolution specular X-ray reflectivity. *J. Synchrotron Radiat.* **13**, 293–303.

Finger L. W. and Hazen R. M. (1980) Crystal structure and isothermal compression of Fe_2O_3, Cr_2O_3, and V_2O_3 to 50 kbars. *J. Appl. Phys.* **51**, 5362–5367.

Gautier-Soyer M., Pollak M., Henriot M. and Guittet M. J. (1996) The (1×2) reconstruction of the α-Fe_2O_3 ($\bar{1}012$) surface. *Surf. Sci.* **352**, 112–116.

Grant M. and Jordan R. B. (1981) Kinetics of solvent water exchange on iron(III). *Inorg. Chem.* **20**, 55–60.

Hayes K. F. and Leckie J. O. (1987) Modeling ionic strength effects on cation adsorption at hydrous oxide/solution interfaces. *J. Colloid Interface Sci.* **115**, 564–572.

Hayes K. F., Papelis C. and Leckie J. O. (1988) Modeling ionic strength effects on anion adsorption at hydrous oxide/solution interfaces. *J. Colloid Interface Sci.* **125**, 717–726.

Henderson M. A., Joyce S. A. and Rustad J. R. (1998) Interaction of water with the (1×1) and (2×1) surfaces of α-Fe_2O_3(012). *Surf. Sci.* **417**, 66–81.

Henderson M. A. (2002) Insights into the (1×1)-to-(2×1) phase transition of the α-Fe_2O_3(012) surface using EELS, LEED and water TPD. *Surf. Sci.* **515**, 253–262.

Hiemstra T. and van Riemsdijk W. H. (1996) A surface structural approach to ion adsorption: the charge distribution (CD) model. *J. Colloid Interface Sci.* **179**, 488–508.

Hiemstra T., van Riemsdijk W. H. and Bolt G. H. (1989) Multisite proton adsorption modeling at the solid/solution interface of (hydr)oxides: a new approach I. Model description and evaluation of intrinsic reaction constants. *J. Colloid Interface Sci.* **133**, 91–104.

Hiemstra T., Venema P. and van Riemsdijk W. H. (1996) Intrinsic proton affinity of reactive surface groups of metal (hydr)oxides: the bond valence principle. *J. Colloid Interface Sci.* **184**, 680–692.

Hsu T. and Kim Y. T. (1991a) Reconstruction of the α-Al_2O_3 $(11\bar{2}0)$ surfaces. *Surf. Sci.* **243**, L63–L66.

Hsu T. and Kim Y. (1991b) Structure of the α-$Al_2O_3(11\bar{2}0)$ surfaces: facets and reconstruction. *Surf. Sci.* **258**, 119–130.

Hugi-Cleary D., Helm L. and Merbach A. E. (1985) Variable-temperature and variable-pressure ^{17}O-NMR study of water exchange of hexaaquaaluminum(III). *Helv. Chim. Acta* **68**, 545–554.

Hura G., Sorenson J. M., Glaeser R. M. and Head-Gordon T. (2000) A high-quality X-ray scattering experiment on liquid water at ambient conditions. *J. Chem. Phys.* **113**, 9140–9148.

Ishizawa N., Miyata T., Minato I., Marúmo F. and Iwai S. (1980) A structural investigation of α-Al_2O_3 at 2170 K. *Acta Crystallogr.* **B36**, 228–230.

Israelachvili J. N. and Pashley R. M. (1983) Molecular layering of water at surfaces and origin of repulsive hydration forces. *Nature* **306**, 249–250.

Lo C. S., Tanwar K. S., Chaka A. M. and Trainor T. P. (2007) Density functional theory study of the clean and hydrated hematite $(1\bar{1}02)$ surfaces. *Phys. Rev. B* **75**, 075425.

Machesky M. L., Wesolowski D. J., Palmer D. A. and Ridley M. K. (2001) On the temperature dependence of intrinsic surface protonation equilibrium constants: an extension of the revised MUSIC model. *J. Colloid Interface Sci.* **239**, 314–327.

Munkholm A. and Brennan S. (1999) Influence of miscut on crystal truncation rod scattering. *J. Appl. Crystallogr.* **32**, 143–153.

Nordin J. P., Sullivan D. J., Phillips B. L. and Casey W. H. (1998) An ^{17}O-NMR study of the exchange of water on $AlOH(H_2O)_5^{2+}$(aq). *Inorg. Chem.* **37**, 4760–4763.

Park C. Y., Fenter P., Zhang Z., Cheng L. W. and Sturchio N. C. (2004) Structure of the fluorapatite (100)–water interface by high-resolution X-ray reflectivity. *Am. Miner.* **89**, 1647–1654.

Park C., Fenter P. A., Nagy K. L. and Sturchio N. C. (2006) Hydration and distribution of ions at the mica–water interface. *Phys. Rev. Lett.* **97**, 016101.

Pflanz S., Meyerheim H. L., Moritz W., Robinson I. K., Hoernis H. and Conrad E. H. (1995) Anisotropic roughening of vicinally miscut Ag(110): X-ray-reflection profile analysis using the domain-matrix method. *Phys. Rev. B* **52**, 2914–2926.

Phillips B. L., Casey W. H. and Karlsson M. (2000) Bonding and reactivity at oxide mineral surfaces from model aqueous complexes. *Nature* **404**, 379–382.

Phillips B. L., Lee A. and Casey W. H. (2003) Rates of oxygen exchange between the $Al_2O_8Al_{28}(OH)_{56}(H_2O)_{26}^{18+}$(aq) ($Al_{30}$) molecule and aqueous solution. *Geochim. Cosmochim. Acta* **67**, 2725–2733.

Robinson I. K. (1986) Crystal truncation rods and surface roughness. *Phys. Rev. B* **33**, 3830–3836.

Schlegel M. L., Nagy K. L., Fenter P. and Sturchio N. C. (2002) Structures of quartz $(10\bar{1}0)$– and $(10\bar{1}1)$–water interfaces determined by X-ray reflectivity and atomic force microscopy of natural growth surfaces. *Geochim. Cosmochim. Acta* **66**, 3037–3054.

Schlegel M. L., Nagy K. L., Fenter P., Cheng L., Sturchio N. C. and Jacobsen S. D. (2006) Cation sorption on the muscovite (001) surface in chloride solutions using high-resolution X-ray reflectivity. *Geochim. Cosmochim. Acta* **70**, 3549–3565.

Schneppensieper T., Seibig S., Zahl A., Tregloan P. and van Eldik R. (2001) Influence of chelate effects on the water-exchange mechanism of polyaminecarboxylate complexes of iron(III). *Inorg. Chem.* **40**, 3670–3676.

Sorenson J. M., Hura G., Glaeser R. M. and Head-Gordon T. (2000) What can X-ray scattering tell us about the radial distribution functions of water? *J. Chem. Phys.* **113**, 9149–9161.

Sverjensky D. A. (1993) Physical surface-complexation models for sorption at the mineral–water interface. *Nature* **364**, 776–780.

Sverjensky D. A. (2001) Interpretation and prediction of triple-layer model capacitances and the structure of the oxide–electrolyte–water interface. *Geochim. Cosmochim. Acta* **65**, 3643–3655.

Tanwar K. S., Lo C. S., Eng P. J., Catalano J. G., Walko D. A., Brown, Jr., G. E., Waychunas G. A., Chaka A. M. and Trainor T. P. (2007a) Surface diffraction study of the hydrated hematite $(1\bar{1}02)$ surface. *Surf. Sci.* **601**, 460–474.

Tanwar K. S., Catalano J. G., Pettito S. C., Ghose S. K., Eng P. J. and Trainor T. P. (2007b) Hydrated α-Fe_2O_3 $(1\bar{1}02)$ surface structure: role of surface preparation. *Surf. Sci.* **601**, L59–L64.

Trainor T. P., Eng P. J., Brown, Jr., G. E., Robinson I. K. and De Santis M. (2002) Crystal truncation rod diffraction study of the α-Al_2O_3 $(1\bar{1}02)$ surface. *Surf. Sci.* **496**, 238–250.

Trainor T. P., Chaka A. M., Eng P. J., Newville M., Waychunas G. A., Catalano J. G. and Brown, Jr., G. E. (2004) Structure and reactivity of the hydrated hematite (0001) surface. *Surf. Sci.* **573**, 204–224.

Waseda Y. (1984) *Novel Application of Anomalous (Resonance) X-ray Scattering for Structural Characterization of Disordered Materials*. Springer-Verlag, New York.

Waychunas G., Trainor T., Eng P., Catalano J., Brown G., Davis J., Rogers J. and Bargar J. (2005) Surface complexation studied via combined grazing-incidence EXAFS and surface diffraction: arsenate an hematite (0001) and (10–12). *Anal. Bioanal. Chem.* **383**, 12–27.

Zhang Z., Fenter P., Cheng L., Sturchio N. C., Bedzyk M. J., Predota M., Bandura A., Kubicki J. D., Lvov S. N., Cummings P. T., Chialvo A. A., Ridley M. K., Benezeth P., Anovitz L., Palmer D. A., Machesky M. L. and Wesolowski D. J. (2004) Ion adsorption at the rutile–water interface: linking molecular and macroscopic properties. *Langmuir* **20**, 4954–4969.

Zhang Z., Fenter P., Kelly S. D., Catalano J. G., Bandura A. V., Kubicki J. D., Sofo J. O., Wesolowski D. J., Machesky M. L., Sturchio N. C. and Bedzyk M. J. (2006a) Structure of hydrated Zn^{2+} at the rutile TiO_2 (110)–aqueous solution interface: comparison of X-ray standing wave, X-ray absorption spectroscopy, and density functional theory results. *Geochim. Cosmochim. Acta* **70**, 4039–4056.

Zhang Z., Fenter P., Cheng L., Sturchio N. C., Bedzyk M. J., Machesky M. L., Anovitz L. M. and Wesolowski D. J. (2006b) Zn^{2+} and Sr^{2+} adsorption at the TiO_2 (110)–electrolyte interface: influence of ionic strength, coverage, and anions. *J. Colloid Interface Sci.* **295**, 50–64.

Associate editor: William H. Casey